PhD Thesis

PhD Thesis
this is a subtitle

by Oliver Matonoha

LUND
UNIVERSITY

Thesis for the degree of Doctorate
Thesis advisors: Prof. Doktor Professorsson, Prof. Knirk Gnork
Faculty opponent: Prof. Gammal och Grå

To be presented, with the permission of the Faculty of Natural Sciences of Lund University, for public criticism at LINXS (Delta 5, floor 5, IDEON building) on friday, the 30th of October 2023 at 10:15.

Organization	Document name
LUND UNIVERSITY Department of Physics Box 124 SE–221 00 LUND Sweden	**LICENTIATE THESIS** Date of disputation 2020-10-30 Sponsoring organization
Author(s) Oliver Matonoha	

Title and subtitle
PhD Thesis this is a subtitle

Abstract
Lorem ipsum dolor sit amet, consectetuer adipiscing elit. Etiam lobortis facilisis sem. Nullam nec mi et neque pharetra sollicitudin. Praesent imperdiet mi nec ante. Donec ullamcorper, felis non sodales commodo, lectus velit ultrices augue, a dignissim nibh lectus placerat pede. Vivamus nunc nunc, molestie ut, ultricies vel, semper in, velit. Ut porttitor. Praesent in sapien. Lorem ipsum dolor sit amet, consectetuer adipiscing elit. Duis fringilla tristique neque. Sed interdum libero ut metus. Pellentesque placerat. Nam rutrum augue a leo. Morbi sed elit sit amet ante lobortis sollicitudin. Praesent blandit blandit mauris. Praesent lectus tellus, aliquet aliquam, luctus a, egestas a, turpis. Mauris lacinia lorem sit amet ipsum. Nunc quis urna dictum turpis accumsan semper.

Key words
quantum chromodynamics, quark-gluon plasma

Classification system and/or index terms (if any)

Supplementary bibliographical information		Language English
ISSN and key title		ISBN 123456789 (print) 123456789 (pdf)
Recipient's notes	Number of pages 83	Price
	Security classification	

PhD Thesis
this is a subtitle

by Oliver Matonoha

LUND
UNIVERSITY

A licentiate thesis at a university in Sweden takes either the form of a single, cohesive research study (monograph) or a summary of research papers (compilation thesis), which the licentiate student has written alone or together with one or several other author(s).

In the latter case the thesis consists of two parts. An introductory text puts the research work into context and summarizes the main points of the papers. Then, the research publications themselves are reproduced, together with a description of the individual contributions of the authors. The research papers may either have been already published or are manuscripts at various stages (in press, submitted, or in draft).

Cover illustration front: Cool figure by bla and bla.

Cover illustration back: Another cool image by bla.

Funding information: The thesis work was financially supported by the Swedish Research Council.

Faculty of Natural Sciences, Department of Physics

ISBN: 123456789 (print)
ISBN: 123456789 (pdf)

Printed in Sweden by Media-Tryck, Lund University, Lund 2023

Media-Tryck is a Nordic Swan Ecolabel certified provider of printed material. Read more about our environmental work at www.mediatryck.lu.se

MADE IN SWEDEN

Dedicated to
Humpty – Dumpty
bla bla blat

Contents

List of publications

This thesis is based on the following publications, referred to by their Roman numerals:

I **Title paper 1**

S. Doctor, B. Someone
The Journal of Physical Chemistry A, 2020, 124(19), pp. 3943-3946

II **Title paper 2**

S. Doctor, B. Someone, C Another
Physical Chemistry Chemical Physics, 2020, 22(24), pp. 13659-13665

All papers are reproduced with permission of their respective publishers.

Acknowledgements

Lorem ipsum dolor sit amet, consectetuer adipiscing elit. Etiam lobortis facilisis sem. Nullam nec mi et neque pharetra sollicitudin. Praesent imperdiet mi nec ante. Donec ullamcorper, felis non sodales commodo, lectus velit ultrices augue, a dignissim nibh lectus placerat pede. Vivamus nunc nunc, molestie ut, ultricies vel, semper in, velit. Ut porttitor. Praesent in sapien. Lorem ipsum dolor sit amet, consectetuer adipiscing elit. Duis fringilla tristique neque. Sed interdum libero ut metus. Pellentesque placerat. Nam rutrum augue a leo. Morbi sed elit sit amet ante lobortis sollicitudin. Praesent blandit blandit mauris. Praesent lectus tellus, aliquet aliquam, luctus a, egestas a, turpis. Mauris lacinia lorem sit amet ipsum. Nunc quis urna dictum turpis accumsan semper.

Populärvetenskaplig sammanfattning på svenska

Lorem ipsum dolor sit amet, consectetuer adipiscing elit. Etiam lobortis facilisis sem. Nullam nec mi et neque pharetra sollicitudin. Praesent imperdiet mi nec ante. Donec ullamcorper, felis non sodales commodo, lectus velit ultrices augue, a dignissim nibh lectus placerat pede. Vivamus nunc nunc, molestie ut, ultricies vel, semper in, velit. Ut porttitor. Praesent in sapien. Lorem ipsum dolor sit amet, consectetuer adipiscing elit. Duis fringilla tristique neque. Sed interdum libero ut metus. Pellentesque placerat. Nam rutrum augue a leo. Morbi sed elit sit amet ante lobortis sollicitudin. Praesent blandit blandit mauris. Praesent lectus tellus, aliquet aliquam, luctus a, egestas a, turpis. Mauris lacinia lorem sit amet ipsum. Nunc quis urna dictum turpis accumsan semper.

PhD Thesis this is a subtitle

Part I

Research motivation

Chapter 1

Introduction to quantum chromodynamics

Lorem ipsum dolor sit amet, consectetuer adipiscing elit. Etiam lobortis facilisis sem. Nullam nec mi et neque pharetra sollicitudin. Praesent imperdiet mi nec ante. Donec ullamcorper, felis non sodales commodo, lectus velit ultrices augue, a dignissim nibh lectus placerat pede. Vivamus nunc nunc, molestie ut, ultricies vel, semper in, velit. Ut porttitor. Praesent in sapien. Lorem ipsum dolor sit amet, consectetuer adipiscing elit. Duis fringilla tristique neque. Sed interdum libero ut metus. Pellentesque placerat. Nam rutrum augue a leo. Morbi sed elit sit amet ante lobortis sollicitudin. Praesent blandit blandit mauris. Praesent lectus tellus, aliquet aliquam, luctus a, egestas a, turpis. Mauris lacinia lorem sit amet ipsum. Nunc quis urna dictum turpis accumsan semper. page[1]. Extra text[1]

[1]to optimize page space

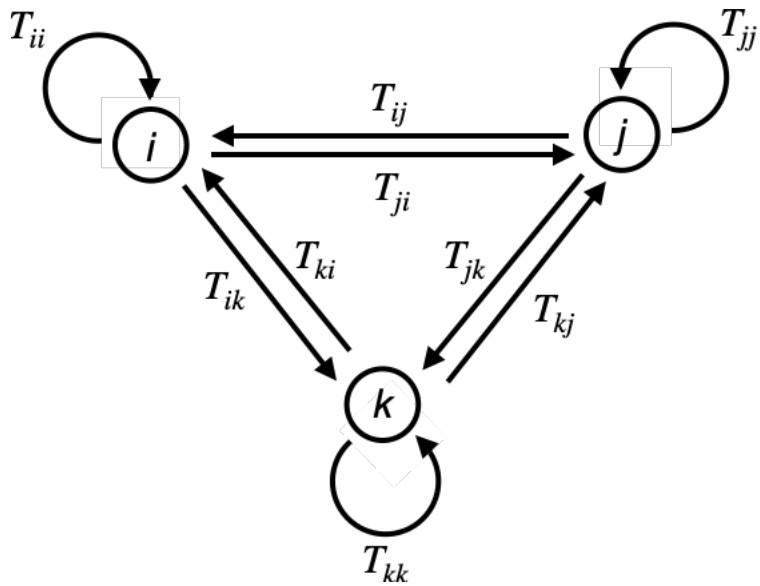

Figure 1.1: Caption

Chapter 2

Collisions of particles at high energies

example 1: Title of Example

Hi, i am a yellow example

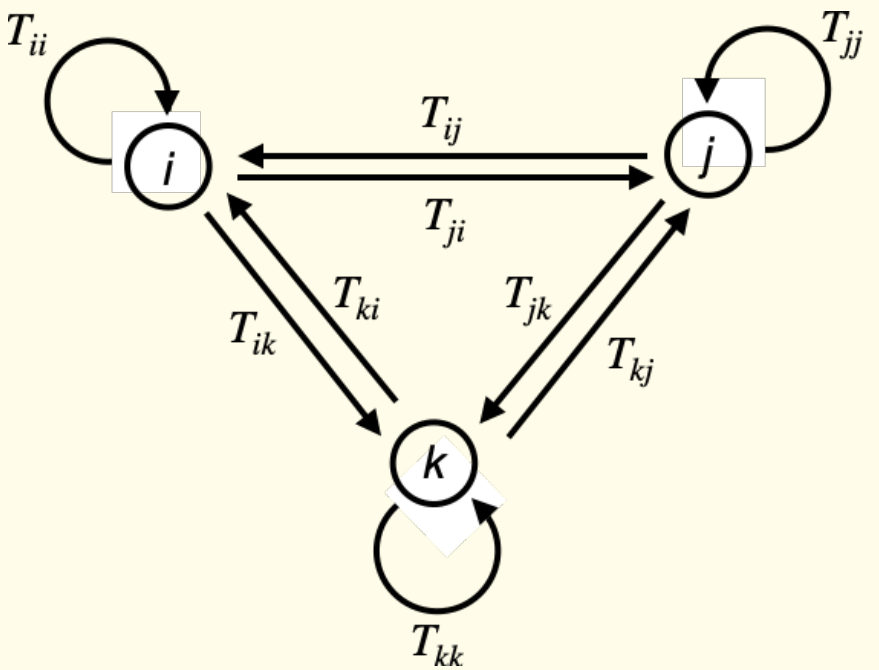

In example 2

The important concept

> Lorem ipsum dolor sit amet, consectetuer adipiscing elit. Etiam lobortis facilisis sem. Nullam nec mi et neque pharetra sollicitudin. Praesent imperdiet mi nec ante. Donec ullamcorper, felis non sodales commodo, lectus velit ultrices augue, a dignissim nibh lectus placerat pede. Vivamus nunc nunc, molestie ut, ultricies vel, semper in, velit. Ut porttitor. Praesent in sapien. Lorem ipsum dolor sit amet, consectetuer adipiscing elit. Duis fringilla tristique neque. Sed interdum libero ut metus. Pellentesque placerat. Nam rutrum augue a leo. Morbi sed elit sit amet ante lobortis sollicitudin. Praesent blandit blandit mauris. Praesent lectus tellus, aliquet aliquam, luctus a, egestas a, turpis. Mauris lacinia lorem sit amet ipsum. Nunc quis urna dictum turpis accumsan semper.

Lorem ipsum dolor sit amet, consectetuer adipiscing elit. Etiam lobortis facilisis sem. Nullam nec mi et neque pharetra sollicitudin. Praesent imperdiet mi nec ante. Donec ullamcorper, felis non sodales commodo, lectus velit ultrices augue, a dignissim nibh lectus placerat pede. Vivamus nunc nunc, molestie ut, ultricies vel, semper in, velit. Ut porttitor. Praesent in sapien. Lorem ipsum dolor sit amet, consectetuer adipiscing elit. Duis fringilla tristique neque. Sed interdum libero ut metus. Pellentesque placerat. Nam rutrum augue a leo. Morbi sed elit sit amet ante lobortis sollicitudin. Praesent blandit blandit mauris. Praesent lectus tellus, aliquet aliquam, luctus a, egestas a, turpis. Mauris lacinia lorem sit amet ipsum. Nunc quis urna dictum turpis accumsan semper.

Chapter 3

QCD phenomena in high energy collisions

Lorem ipsum dolor sit amet, consectetuer adipiscing elit. Etiam lobortis facilisis sem. Nullam nec mi et neque pharetra sollicitudin. Praesent imperdiet mi nec ante. Donec ullamcorper, felis non sodales commodo, lectus velit ultrices augue, a dignissim nibh lectus placerat pede. Vivamus nunc nunc, molestie ut, ultricies vel, semper in, velit. Ut porttitor. Praesent in sapien. Lorem ipsum dolor sit amet, consectetuer adipiscing elit. Duis fringilla tristique neque. Sed interdum libero ut metus. Pellentesque placerat. Nam rutrum augue a leo. Morbi sed elit sit amet ante lobortis sollicitudin. Praesent blandit blandit mauris. Praesent lectus tellus, aliquet aliquam, luctus a, egestas a, turpis. Mauris lacinia lorem sit amet ipsum. Nunc quis urna dictum turpis accumsan semper.

Chapter 4

Phenomenological models of hadronic collisions

Lorem ipsum dolor sit amet, consectetuer adipiscing elit. Etiam lobortis facilisis sem. Nullam nec mi et neque pharetra sollicitudin. Praesent imperdiet mi nec ante. Donec ullamcorper, felis non sodales commodo, lectus velit ultrices augue, a dignissim nibh lectus placerat pede. Vivamus nunc nunc, molestie ut, ultricies vel, semper in, velit. Ut porttitor. Praesent in sapien. Lorem ipsum dolor sit amet, consectetuer adipiscing elit. Duis fringilla tristique neque. Sed interdum libero ut metus. Pellentesque placerat. Nam rutrum augue a leo. Morbi sed elit sit amet ante lobortis sollicitudin. Praesent blandit blandit mauris. Praesent lectus tellus, aliquet aliquam, luctus a, egestas a, turpis. Mauris lacinia lorem sit amet ipsum. Nunc quis urna dictum turpis accumsan semper.

Part II

Experimental Setup and Methodology

Chapter 5

Large Hadron Collider

5.1 European Organisation for Nuclear Research

CERN, located near Geneva, Switzerland, is an esteemed scientific institution dedicated to the study of particle physics, nuclear physics, and related fields. Established in 1954 by a consortium of European countries, it currently has 23 member states and collaborates with over 50 countries worldwide. Its research endeavors focus on advancing our understanding of the fundamental particles and forces that govern them.

One of the most significant and celebrated discoveries made by CERN is the Higgs boson, a particle that confers mass to other particles and is a crucial component of the Standard Model of particle physics. This discovery was made in 2012 by the ATLAS and CMS experiments, two of the four main experiments at CERN's Large Hadron Collider (LHC), the world's largest and most powerful particle accelerator.

Apart from the LHC, CERN houses several research facilities, including the Proton Synchrotron and the Super Proton Synchrotron, that provide beams of particles for a wide range of experiments.

5.2 Large Hadron Collider (LHC)

The Large Hadron Collider (LHC) is a particle accelerator that utilizes a circular tunnel with a circumference of 27 kilometers to accelerate beams of protons or heavy ions to high energies and collide them at four separate experimental locations. The LHC operates on the principle of accelerating these beams to nearly the speed of light

through a series of superconducting magnets and then directing them to collide with each other at specific points along the circular path.

The LHC's superconducting magnets are cooled to temperatures close to absolute zero (-271.3 degrees Celsius) to maintain their superconducting state, allowing them to guide and focus the particle beams as they travel along the circular path. These magnets produce a strong magnetic field that keeps the particle beams on their circular trajectory and causes them to bend as they pass through the magnetic field. By adjusting the strength of the magnetic field, the LHC can control the curvature of the particle beams and ensure that they collide at the designated interaction points.

The LHC's acceleration process occurs in a series of stages, starting with a source of particles that are injected into a linear accelerator (LINAC). The LINAC accelerates the particles to an energy of a few million electronvolts (MeV) before passing them to a circular accelerator called a Booster. The Booster further accelerates the particles to an energy of 1.4 billion electronvolts (GeV) before injecting them into the Proton Synchrotron (PS).

The PS is a circular accelerator that increases the energy of the particles to 25 GeV before injecting them into the Super Proton Synchrotron (SPS). The SPS is a larger circular accelerator that further accelerates the particles to 450 GeV before finally injecting them into the LHC. Once inside the LHC, the particles are accelerated to their final energy and directed to collide at the designated interaction points.

The collisions at the LHC produce a shower of subatomic particles that are captured and analyzed by the LHC's four primary detectors: ATLAS, CMS, LHCb, and ALICE. These detectors are designed to measure the properties and trajectories of the particles produced by the collisions and provide valuable insights into the fundamental nature of matter and the universe.

Overall, the operational principle of the LHC is based on the precise control of the particle beams through a series of superconducting magnets and accelerators to produce high-energy collisions that enable cutting-edge research in particle physics.

The LHC tunnel is situated approximately 100 meters underground, in a tunnel that was previously used by the Large Electron-Positron Collider (LEP). It has a diameter of 3.8 meters and houses over 1,600 superconducting magnets. The collider operates for periods of several months at a time, with periods of downtime in between for maintenance and upgrades.

TBA Luminosity, bunches, Van der Meer scans

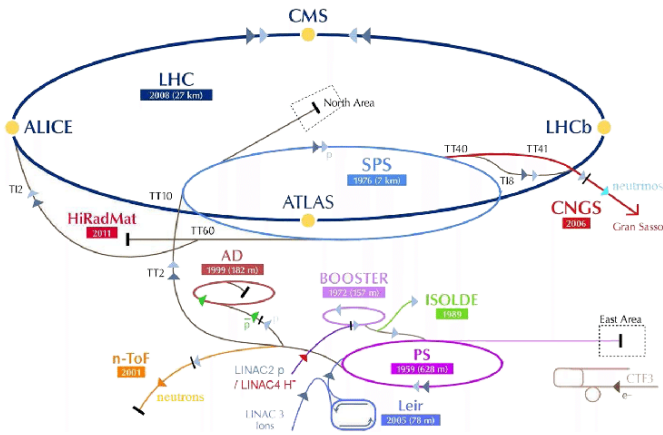

Figure 5.1: TBA.

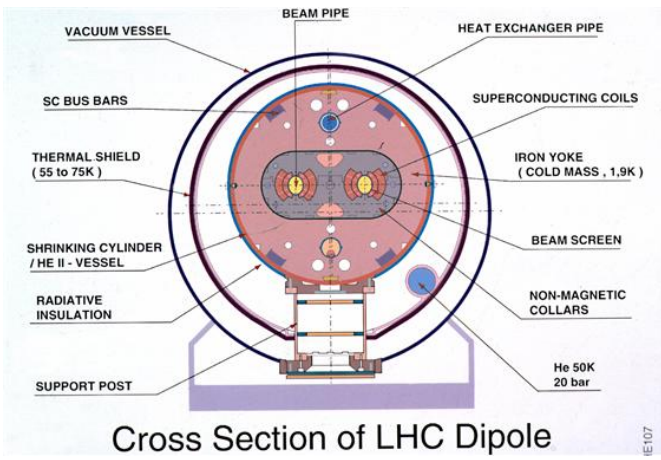

Figure 5.2: TBA.

Chapter 6

The ALICE Detector

The ALICE (A Large Ion Collider Experiment) is one of four major detectors located at the Large Hadron Collider (LHC) at CERN. The ALICE detector is designed to study the properties of the quark-gluon plasma (QGP), a state of matter that existed a few microseconds after the Big Bang.

The ALICE detector consists of several sub-detectors that work together to capture and analyze the particles produced by the collisions at the LHC. The central component of the ALICE detector is the Time Projection Chamber (TPC), a large cylinder filled with a gas mixture that is used to detect the charged particles produced by the

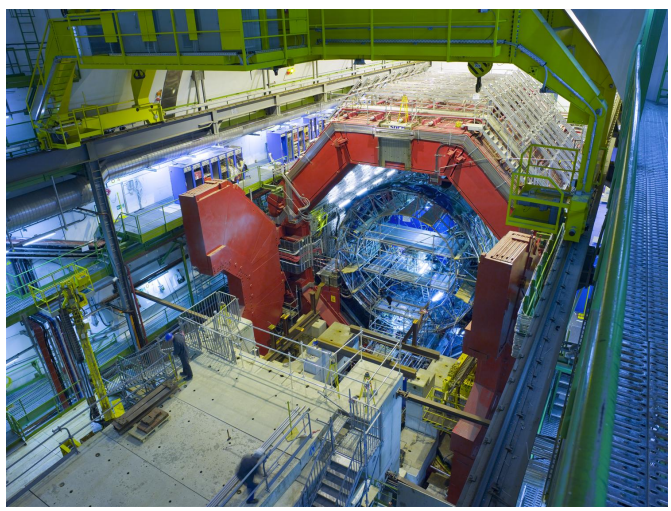

Figure 6.1: TBA.

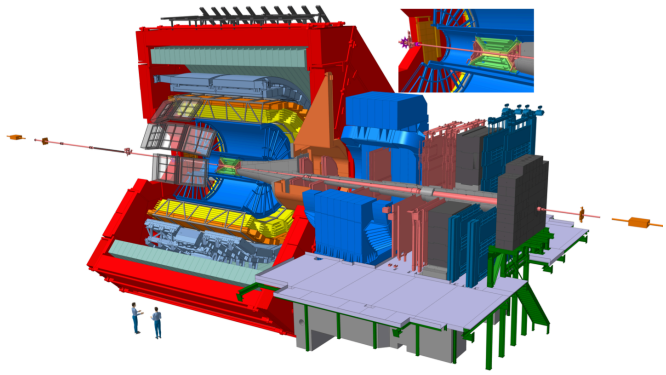

Figure 6.2: TBA.

collisions. The TPC measures the position, momentum, and energy of the particles, allowing scientists to reconstruct their trajectories and identify the different particle species.

In addition to the TPC, the ALICE detector also includes several other sub-detectors, such as the Inner Tracking System (ITS), the Transition Radiation Detector (TRD), and the Time-Of-Flight (TOF) detector. The ITS is a high-precision tracking detector that is used to measure the trajectories of charged particles produced in the collisions. The TRD is used to identify electrons and measure their energy. The TOF detector measures the time-of-flight of particles and is used to determine their momentum.

6.1 Time Projection Chamber

The TPC works by filling the cylinder with a gas, typically a mixture of helium and carbon dioxide, and applying an electric field to create a uniform drift velocity for the charged particles. As the particles move through the gas, they ionize the atoms, creating free electrons and ions. The electrons are then attracted to a central anode, where they are detected and used to reconstruct the particle tracks.

The TPC has a number of advantages over other types of detectors. For one, it is able to provide precise measurements of the position and momentum of the charged particles, which allows scientists to study the behavior of quark-gluon plasma and other forms of matter at extremely high temperatures and densities. The TPC is also able to reconstruct the tracks of thousands of particles produced in a single collision, which provides a comprehensive view of the event.

The TPC in the ALICE experiment is particularly advanced, with over 500,000 read-

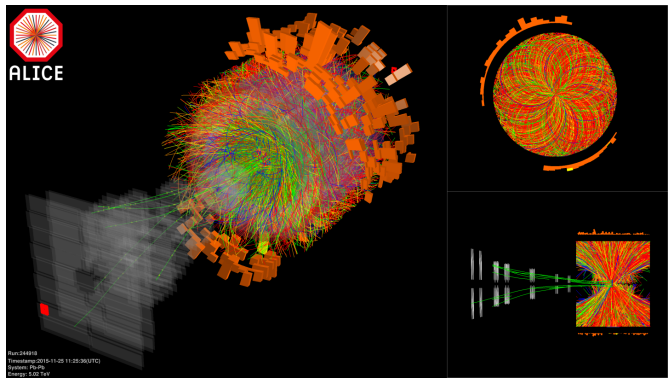

Figure 6.3: TBA.

out channels and a sensitive volume of over 90 cubic meters. It is able to operate at high collision rates, with a maximum readout rate of 50 kHz. The TPC also has a number of innovative features, such as a gating system that allows the detector to operate in the presence of large magnetic fields, and a continuous calibration system that ensures high data quality.

6.2 Inner Tracking Systems

The ITS is another tracking detector in the ALICE experiment, located closer to the collision point than the TPC. It is designed to provide precise measurements of the position of charged particles as they are produced in the collisions. The ITS consists of six layers of silicon detectors, which provide high-resolution measurements of the position and momentum of the particles. The ITS is particularly useful for studying the very early stages of the collision, where the particles are produced in a very small volume and with high energies.

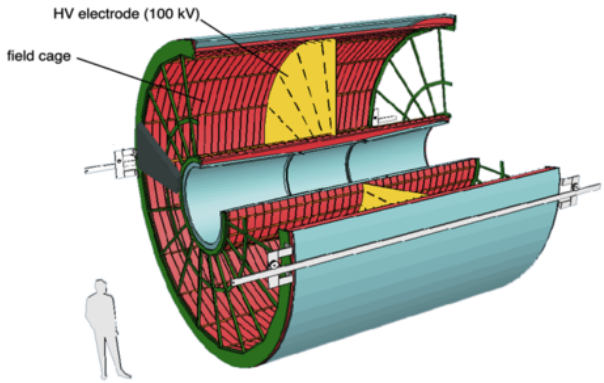

Figure 6.4: TBA.

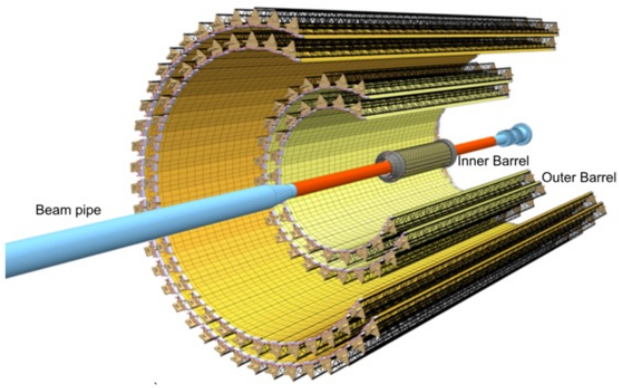

Figure 6.5: TBA.

Chapter 7

Events, Vertices, Tracks, and Particles

Lorem ipsum dolor sit amet, consectetuer adipiscing elit. Etiam lobortis facilisis sem. Nullam nec mi et neque pharetra sollicitudin. Praesent imperdiet mi nec ante. Donec ullamcorper, felis non sodales commodo, lectus velit ultrices augue, a dignissim nibh lectus placerat pede. Vivamus nunc nunc, molestie ut, ultricies vel, semper in, velit. Ut porttitor. Praesent in sapien. Lorem ipsum dolor sit amet, consectetuer adipiscing elit. Duis fringilla tristique neque. Sed interdum libero ut metus. Pellentesque placerat. Nam rutrum augue a leo. Morbi sed elit sit amet ante lobortis sollicitudin. Praesent blandit blandit mauris. Praesent lectus tellus, aliquet aliquam, luctus a, egestas a, turpis. Mauris lacinia lorem sit amet ipsum. Nunc quis urna dictum turpis accumsan semper.

Part III

Author's measurements

Chapter 8

Reconstruction of neutral strange particles with ALICE

Hadrons K^0_S and Λ ($\overline{\Lambda}$) are unstable neutral primary particles that usually decay within the volume of the detector through the weak interaction. Their mean lifetimes are $\sim 2.7\,\mathrm{cm}/c$ and $\sim 7.9\,\mathrm{cm}/c$, respectively.[2] Their dominant decay channels, which are also used for their measurement, are:

$$\mathrm{K}^0_\mathrm{S} \to \pi^+ \pi^- \tag{8.1}$$

$$\Lambda \to p\,\pi^- \tag{8.2}$$

$$\overline{\Lambda} \to \bar{p}\,\pi^+ \ . \tag{8.3}$$

Because of how these hadrons' decay topologies appear in the detector (an undetectable neutral particle decaying into a V-shaped pair of detectable tracks), they are commonly nicknamed V0s[1].

8.1 Analysed datasets

TBA Description of data, collection years, some QA Monte Carlo The Monte Carlo data are simulated using a physics event generator (in this measurement, Pythia 8) and a model describing the propagation of particles through the detector environment (GEANT).

[1] Not to be confused with V0A and V0C—the forward calorimeters in ALICE, or V0M—the related multiplicity estimator using the calorimeters' signal.

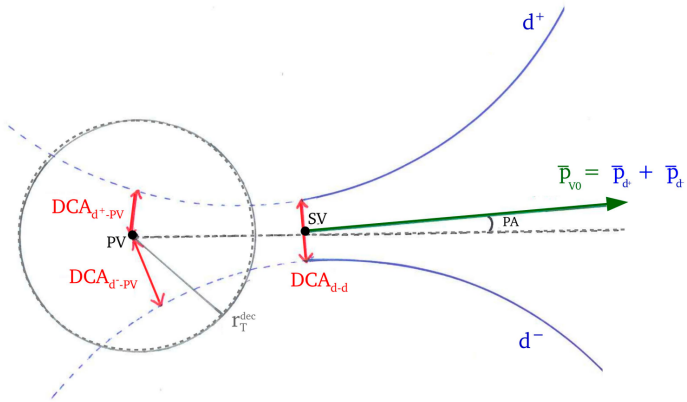

Figure 8.1: Typical topology of V0 decay. PV stands for primary vertex, SV for secondary vertex. ? p. 102

8.2 Identification of V0s using ALICE

A centrally developed ALICE algorithm, the ALICE V0 finder, is used to collect suitable V0 candidates from pairs of oppositely charged tracks with the relevant topology. This typical topology is illustrated in Fig. **??** Additional selection criteria ("cuts") are further applied to suppress the background among those candidates. These include:

- cuts on kinematics of the mother and the daughters,
- constraints on the topology of the decay,
- constraints on the reconstruction quality of the daughter tracks,
- cuts on the specific ionisation energy loss of the daughters,
- rejection of contributions from pile-up using "fast detector" information,
- rejection of other competing V0 candidates based on their invariant mass.

The full list of used cuts is listed in Tab. 8.1.

8.3 Signal extraction

The V0 signal is separated from the background in distributions of M_{inv} in several p_{T} intervals using the so-called sideband method. Assuming the signal peaks around $\Delta m_{\mathrm{V0}} = M_{\mathrm{inv}} - M_{\mathrm{V0}} = 0$ and approximating the background in this region as linear, the subsequent procedure is followed:

Table 8.1: Cuts used in the identification of the K^0_S, Λ, and $\overline{\Lambda}$ particles.

Cut Variable	Cut Value for K^0_S (Λ, $\overline{\Lambda}$)
Topology	
V^0 pseudorapidity	$-0.8 < \eta < 0.8$
Transverse momentum	$1.0 < p_\mathrm{T} < 25.0\ \mathrm{GeV}/c$
V^0 DCA	$\mathrm{DCA}^{\mathrm{d-d}} < 1.0$
Pointing angle	$\cos \mathrm{PA} > 0.97(0.995)$
Decay radius	$0.5\ \mathrm{cm} < R_{xy}$
Daughter Tracks Selection	
DCA of daughters to PV	$\mathrm{DCA}_{xy}^{\mathrm{d-PV}} > 0.06$ cm
TPC PID of daughters	$< 5\,\sigma$
Track pseudorapidity	$-0.8 < \eta < 0.8$
TPC crossed rows	$N_\mathrm{cr} > 70$
TPC crossed rows to findable ratio	$N_\mathrm{cr}/N_\mathrm{f} > 0.8$
Candidate Selection	
Proper lifetime (transverse)	$(\, R_{xy} \times m_{(\Lambda,\overline{\Lambda})}/p_\mathrm{T} < 30\ \mathrm{cm}\,)$
Competing mass	$> 4\,\sigma$

1. the sideband regions are defined. The M_inv spectra are fitted in the $-0.03 < M_\mathrm{inv} < -0.03\,\mathrm{GeV}/c^2$ interval using a χ^2-fit with the distribution

$$f = [0] + [1] \cdot M_\mathrm{inv} + [2] \cdot \mathcal{N}(\mu, \sigma_1^2) + [3] \cdot \mathcal{N}(\mu, \sigma_2^2)\ , \tag{8.4}$$

   where $\mathcal{N}$ is a Gaussian distribution. This is done in all p_T bins and illustrated in Fig. 8.4.

2. In each p_T bin, parameter σ is obtained as the RMS of $[2] \cdot \mathcal{N}(\mu, \sigma_1^2) + [3] \cdot \mathcal{N}(\mu, \sigma_2^2)$. To calculate the RMS, the distribution is sampled 10^5 times.

3. Variables μ_V0 and σ_V0 as functions of p_T are interpolated using χ^2 fit and the parametrisations:

$$\mu_{\mathrm{K}^0_\mathrm{S}}(p_\mathrm{T}) = \begin{cases} [0] + [1] \cdot p_\mathrm{T} + [2] \cdot p_\mathrm{T}^2 & \text{if } p_\mathrm{T} < 1.6\,\mathrm{GeV}/c, \\ [3] & \text{if } p_\mathrm{T} \geq 1.6\,\mathrm{GeV}/c, \end{cases} \tag{8.5}$$

$$\mu_{\Lambda,\overline{\Lambda}}(p_\mathrm{T}) = \begin{cases} [0] + [1] \cdot p_\mathrm{T} + [2] \cdot p_\mathrm{T}^2 & \text{if } p_\mathrm{T} < 1.9\,\mathrm{GeV}/c, \\ [3] + [4] \cdot p_\mathrm{T} & \text{if } p_\mathrm{T} \geq 1.9\,\mathrm{GeV}/c, \end{cases} \tag{8.6}$$

$$\sigma_\mathrm{V0}(p_\mathrm{T}) = [0] + [1] \cdot p_\mathrm{T} + \frac{[2]}{p_\mathrm{T}}\ . \tag{8.7}$$

   The fitted parametrisations can be seen in Fig. 8.3.

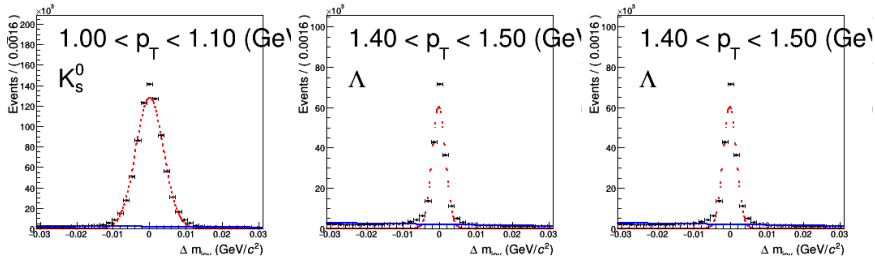

Figure 8.2: Determination of the signal peak mean and width using a fit of the Gaussian distribution for K^0_S, Λ, and $\overline{\Lambda}$ particles.

4. In each p_T bin, we define the signal region **N** as $(\mu_{\mathrm{V0}} - 6\sigma_{\mathrm{V0}}; \mu_{\mathrm{V0}} + 6\sigma_{\mathrm{V0}})$ and the sidebands **A** and **B** as $(\mu_{\mathrm{V0}} - 12\sigma_{\mathrm{V0}}; \mu_{\mathrm{V0}} - 6\sigma_{\mathrm{V0}})$ and $(\mu_{\mathrm{V0}} + 6\sigma_{\mathrm{V0}}; \mu_{\mathrm{V0}} + 12\sigma_{\mathrm{V0}})$. In these regions, we sum together the entries and acquire N, A, B. The choice of $6\sigma_{\mathrm{V0}}$ is rather liberal to avoid biases from incorrect determination of the μ_{V0} or the imperfect description of the signal peak width σ_{V0}

5. Since the background is assumed to be linear, the sum of the two sideband integrals is an accurate estimation of the background in the signal region. Particle yields Y and the corresponding statistical uncertainties σ_Y are calculated as

$$Y = N - A - B \tag{8.8}$$

$$\sigma_Y = \sqrt{N + A + B}\ , \tag{8.9}$$

due to the fact that the statistical uncertainties in the signal and sideband regions are fully uncorrelated. Illustrations of this step can be seen in Fig. **??**.

8.3.1 Validation using simulations

The accuracy of the sideband method is tested with "MC closure"—in MC simulated data, the p_T-spectra acquired blindly from the V0 candidates are compared with p_T-spectra of identified V0. The ratios can be seen in Fig. **??** and show a $\sim 5\%$ effect at high-p_T. This is caused by the fact that in ALICE MC simulations, the V0 mass peaks have somewhat longer tails than in data and thus the signal can enter the background regions. This has to be taken into account when defining reconstruction efficiency using MC data.

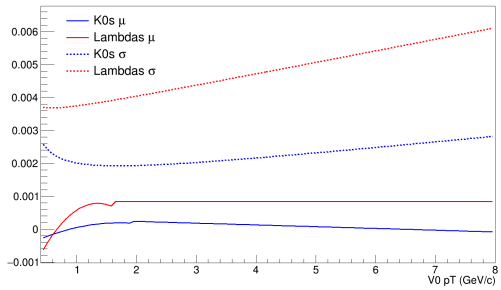

Figure 8.3: Parametrisation of the signal peak mean and width as a function of p_{T}.

Alternative approach

Originally, methods involving a likelihood fit and an unbinned likelihood fit of two Gaussian distributions as well as other background descriptions were tested. However, although more sophisticated, these methods proved considerably less precise. This is due to the fact that the signal peaks cannot be accurately described by the two Gaussian distributions, particularly in highly populated p_{T} bins. That said, they are sufficient to determine the σ_{V0} for above-stated purposes.

Mass resolution of secondary Λ and $\overline{\Lambda}$ particles

Approximately 20% of the Λ yields measured are produced as secondary particles coming from decays of the Ξ baryon in most cases – also called feeddown. Investigations of the simulated data revealed that the invariant mass of these secondaries suffers from a worse resolution (ca. 3 times higher σ). Subsequently, this gives our signal extraction a ca. 75% efficiency for secondaries, and ca. 95% efficiency for inclusive Λ yields at intermediate p_{T}. This has to be taken into consideration when calculating corrections for the feeddown yields. This effect can be seen in Fig. 8.5.

8.4 Normalisation

The reconstructed $\mathrm{K}^0_{\mathrm{S}}$, Λ, and $\overline{\Lambda}$ yields $Y(\eta, p_{\mathrm{T}})$ are normalised according to

$$\frac{\mathrm{d}^2 N^{\mathrm{raw}}}{\mathrm{d}y \mathrm{d}p_{\mathrm{T}}} = \frac{1}{N_{\mathrm{ev}}} \frac{1}{J} \frac{1}{\Delta\eta} \frac{1}{\Delta p_{\mathrm{T}}} Y(\eta, p_{\mathrm{T}}) \quad , \tag{8.10}$$

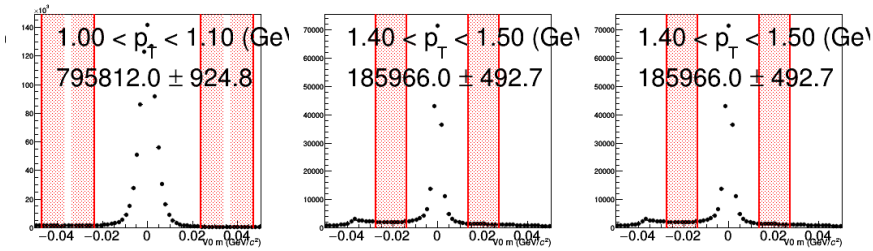

Figure 8.4: Visualisation of the sideband regions, from which the background is estimated, for K^0_S, Λ, and $\overline{\Lambda}$ particles.

where N_ev is the number of selected events, J the Jacobian of the $\eta \to y$ transformation, and $\Delta\eta$ and Δp_T the widths of the pseudorapidity and transverse momentum intervals, respectively.

TBA Jacobian

TBA Event loss correction

8.5 Corrections to the reconstructed production

To acquire results with scientific relevance, the raw yields of V0s observed with ALICE need to be corrected for geometrical acceptance, detector effects, and, in the case of Λ ($\overline{\Lambda}$), also for secondary contribution.

8.5.1 Secondary contribution correction

Only ca. 80% of the measured inclusive Λ and $\overline{\Lambda}$ yields are produced directly in the pp collision or near-instantanously in non-weak decays of resonances, as primary particles. The remainder is produced secondarily, as products of weak decays of heavier baryons. The dominant, and the only relevant, reactions are:

$$\Xi^- \to \Lambda\,\pi^- \ , \tag{8.11}$$

$$\Xi^0 \to \Lambda\,\pi^0 \ , \tag{8.12}$$

$$\Xi^+ \to \overline{\Lambda}\,\pi^+ \ , \tag{8.13}$$

$$\overline{\Xi}^0 \to \overline{\Lambda}\,\pi^0 \ . \tag{8.14}$$

For the K^0_S, the secondary production (such as from ϕ mesons) is negligible.

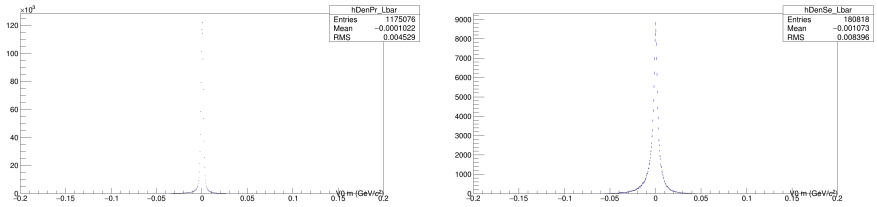

(a) (b)

Figure 8.5: TBA.

The primary Λ yields can be estimated using the following equation,

$$\Lambda^{\mathrm{raw}}_{\mathrm{primary}}(p^i_{\mathrm{T}}) = \Lambda^{\mathrm{raw}}_{\mathrm{measured}} - \Lambda^{\mathrm{raw}}_{\mathrm{secondary}} \tag{8.15}$$

$$= \Lambda^{\mathrm{raw}}_{\mathrm{measured}} - \sum_j F^{\Lambda}_{ij} \int_{p^j_{\mathrm{T}}} \frac{dN}{dp_{\mathrm{T}}}(\Xi^-) \quad , \tag{8.16}$$

where F_{ij} is the so-called feeddown matrix giving the probabilities of a produced Ξ^- or Ξ^0 particle in a p_{T} interval j decaying into reconstructed Λ in a p_{T} interval i, and $\frac{dN}{dp_{\mathrm{T}}}(\Xi^-)$ the measured Ξ^- spectra. This approach assumes that the Ξ^0 decay contribution is identical to Ξ^- and is used because Ξ^0 baryons are challenging to measure. For the $\overline{\Lambda}$, the equation is analogous but uses Ξ^+ .

The feeddown matrix is calculated in ALICE MC simulations of MB events,

$$F^{\Lambda}_{ij} = 2 \cdot \frac{N_{\mathrm{rec.}}(\Lambda)|^{p^{\Xi}_{\mathrm{T}}=j}_{p^{\Lambda}_{\mathrm{T}}=i}}{N_{\mathrm{gen.}}(\Xi)|_{p^{\Xi}_{\mathrm{T}}=j}} \quad , \tag{8.17}$$

where Ξ represent both Ξ^- and Ξ^0. There is an assumption that the probabilities, and thus, the matrix, do not depend on multiplicity of the event. It is taken into account in systematic uncertainties.

An alternative approach is constructing F^{Λ}_{ij} from charged Ξ solely, and then multiplying $\Lambda^{\mathrm{raw}}_{\mathrm{secondary}}$ by two and was used to determine the systematic uncertainty.

As discussed previously, due to the worse mass resolution of secondary Λ, a M_{inv} cut of $5\sigma_{\mathrm{V0}}$ (determined in the sideband definition procedure). Since a large amount of the secondaries enter the background regions, a negative weight -1 has to be applied to achieve the best MC closure validation. Other configurations ($6\sigma_{\mathrm{V0}}$ and -1 weight, $4\sigma_{\mathrm{V0}}$ and 0 weight) were also tested.

The feeddown matrices F^{Λ}_{ij}, $F^{\overline{\Lambda}}_{ij}$ are displayed in Fig. 8.6.

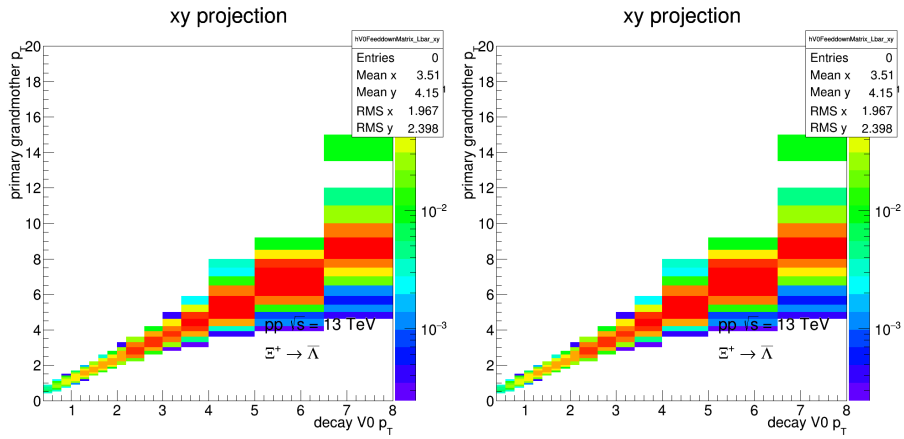

(a) (b)

Figure 8.6: Feeddown matrices **(a)** F_{ij}^{Λ} and **(b)** $F_{ij}^{\overline{\Lambda}}$ from Ξ baryons.

Ξ spectra

Fitting. TBA

8.5.2 Reconstruction efficiency

The total reconstruction efficiency, including the acceptance, for V0s in our events with ALICE can be determined using the Monte Carlo simulated data. It is calculated as

$$\epsilon(p_{\mathrm{T}}) = \text{acceptance} \times \epsilon_{\text{rec}} \tag{8.18}$$

$$= \frac{\#\,\text{associated reconstructed V0s}}{\#\,\text{generated V0s within}\,|\eta| < 0.8}\,, \tag{8.19}$$

in events that passed the selection criteria. The association is done by comparing the mother's and daughters' PDG ID as well as the MC generator label. Particles in the numerator have to satisfy all selection cuts. The reconstruction efficiency for $\mathrm{K}^0_{\mathrm{S}}$, Λ, and $\overline{\Lambda}$ is plotted in Fig. 8.8.

As mentioned before, in ALICE simulations, the M_{inv} resolution worsens with increasing p_{T}; in high-p_{T} bins, the simulated V0s are sometimes reconstructed with higher M_{inv} than what is considered realistic. This would lead to a lower efficiency as those V0s can fall out of the signal region, and an overestimation of the total measured spectra. For this reason, a $4\sigma_{\mathrm{V0}}$ cut is required for the V0s M_{inv} in the numerator.

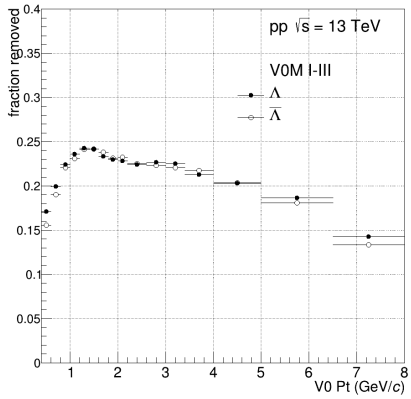

Figure 8.7: TBA.

Alternatively, one could use a cut of $6\sigma_{\mathrm{V0}}$ and applying a negative weight -1 in cases where it is not satisfied.

The reconstruction efficiency is defined in MB events, assuming the reconstruction in pp collisions does not largely depend on multiplicity, geometrical event classification, or event sub-structure. This assumption is taken into account in systematic uncertainties.

8.6 Transverse momentum spectra

Using the corrections on the normalised yields, one acquires the measured transverse momentum spectra, which are comparable with production cross sections and thus theoretical predictions.

$$\frac{\mathrm{d}^2N}{\mathrm{d}y\mathrm{d}p_{\mathrm{T}}} = \epsilon(p_{\mathrm{T}}) \times \frac{\mathrm{d}^2N^{\mathrm{raw}}_{\mathrm{primary}}}{\mathrm{d}y\mathrm{d}p_{\mathrm{T}}} \tag{8.20}$$

8.6.1 Comparisons with previously published results

The acquired results were tested against previously published measurements of $\mathrm{K}^0_{\mathrm{S}}$, Λ, and $\overline{\Lambda}$ transverse momentum spectra at the ALICE experiment in MB as well as high-multiplicity (V0M I and V0M III) events in pp collisions at $\sqrt{s} = 13$ TeV.

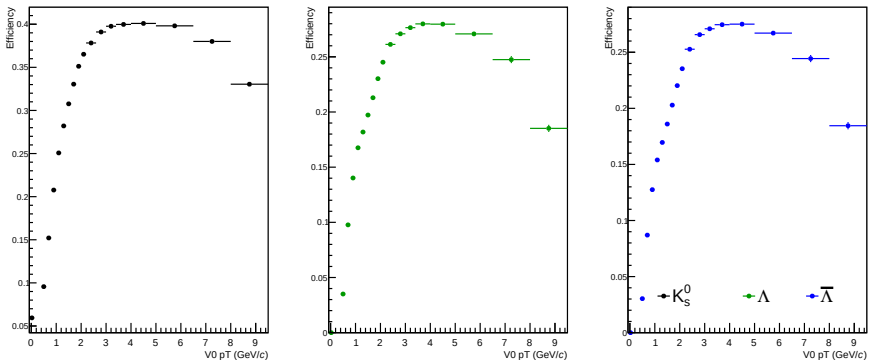

Figure 8.8: TBA.

K^0_S

The published K^0_S results were measured in `kINT7` events. Thus, in order to compare on an equal footing, a trigger efficiency scaling factor $\epsilon_{\text{trig}} = 0.7448$, taken over from, was applied to this analysis.

The comparison of this analysis to the published results can be seen in Fig. 8.9a. In high-multiplicity events, the spectra are in a good agreement across the entire p_{T} range (most points lie within $\sim 5\%$ difference). In MB events, there is a difference ($\sim 10\%$) at the lowest p_{T} values. This is understood as a loss of signal in events with no reconstructed charged tracks and is usually corrected for. Since the correction plays a role only in MB – events which are of little interest to this thesis' work – it is not taken into account.

Λ + $\overline{\Lambda}$

The published Λ + $\overline{\Lambda}$ results were measured in same events as this analysis, (`INEL>0`), therefore, ϵ_{trig} was not applied. They are compared to this analysis in Fig. 8.9b and show a satisfactory agreement (most points lie within $\sim 5\%$ difference).

8.7 Systematic uncertainties

Experimentally measured values always come with uncertainties – statistical and systematic. Whereas statistical uncertainties are caused by the limited number of measurements and can be decreased by increasing the statistical sample analyzed, system-

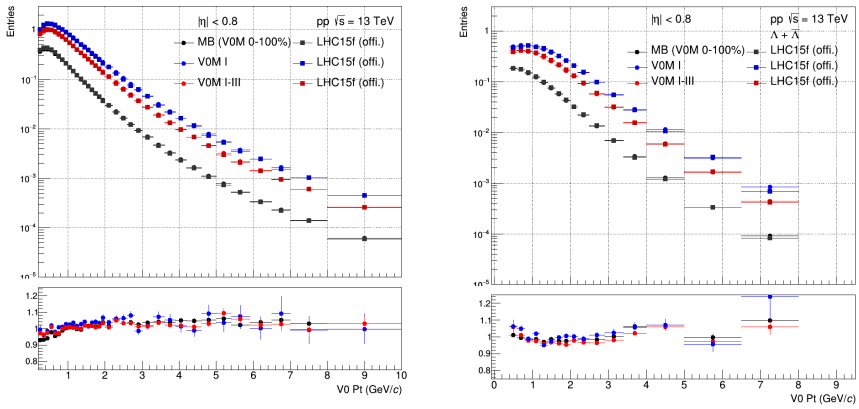

(a) (b)

Figure 8.9: Cross-checks of this analysis' p_{T} spectra of **(a)** $\mathrm{K}^0_{\mathrm{S}}$ and **(b)** $\Lambda + \overline{\Lambda}$ in MB, $\mathrm{V0M}$ I, and $\mathrm{V0M}$ I-III events in pp collisions at against $\sqrt{s} = 13$ TeV results previously published by ALICE.

atic uncertainties represent the imprecision or the bias of the experimental methodology itself. Calculation of statistical uncertainties is given directly from frequentist statistics. Definition of systematic uncertanties, however, is not always straightforward – one cannot simply re-do the measurement with several completely different experimental setups and data analysis techniques. Therefore, a lot of effort needs to go into identifying all possible sources of systematic uncertainties.

In this measurement, the following sources of systematic uncertainty were identified as relevant:

- **Variation of selection criteria**
  In determining the reconstruction efficiency, it is assumed that in ALICE MC simulations, all observables used for the identification of V0s and for assuring the quality of daughter tracks represent reality. Their inaccurate description, however, results in a bias. This bias is estimated by testing the sensitivity of the final results to varying the selection criteria on these observables.

- **Signal extraction method**
  The biases of the sideband background estimation procedure are tested against increasing and reducing the signal and background regions, by varying the number of σ_{V0}. Variations of 5 and 7 σ_{V0} were used.

- **Multiplicity dependence of $\epsilon(p_{\mathrm{T}})$**
  Studies of the reconstruction efficiency in pp collisions reveal a small, albeit

significant dependence on the collision final state. A constant uncertainty of $\sim 2\%$ is applied on the spectra to account for this.

- **Feeddown correction**
  Three sources of uncertainty on the contribution of secondary particles were identified – variation of the Ξ yields, multiplicity dependence of the feeddown matrix, and an alternative method.

- **Material budget**
  This uncertainty reflects that implementing ALICE's material composition in simulations comes with limitations. Previous studies in ALICE which varied parameters of the description of the apparatus showed that this effect corresponds to a constant 4% uncertainty on the measured spectra.

When testing the default method A against an alternative method B, one can implement the deviation of the ratio of their measured values $\Delta = B/A$ from unity as an uncertainty. To ensure that this difference is statistically significant and not just an effect of a limited data sample, the deviation is considered only if it exceeds its own uncertainty, defined as

$$\sigma_\Delta = \frac{\sqrt{|\sigma_B^2 - \sigma_A^2|}}{A} \quad , \tag{8.21}$$

where σ_A and σ_B are the uncertainties of the results from methods A and B, respectively.

8.7.1 Variation of selection criteria

To investigate the differences between description of variables in measured data and ALICE simulations, and determine sensible cut variations λ_i, raw yield loss F was studied. It was measured in MB events and defined as

$$F(\lambda) = 1 - \frac{Y(\lambda)}{Y(\lambda_0)} \quad , \tag{8.22}$$

where $Y(\lambda)$ is the raw yield as a function of the cut value λ and $\lambda_{\mathrm{LOOSEST}}$ the loosest variation (corresponding to the highest yield).

For most observables, the systematic effect can be estimated from alternative methods using $\lambda_{\mathrm{LOOSEST}}$ and $\lambda_{\mathrm{TIGHTEST}}$. To ensure the stability and possible non-linearity, less strict λ_{LOOSE} and λ_{TIGHT} are also tested. If applicable t is reasonable to choose λ_i such that $F(\lambda_i)$ does not exceed approximately 10%.

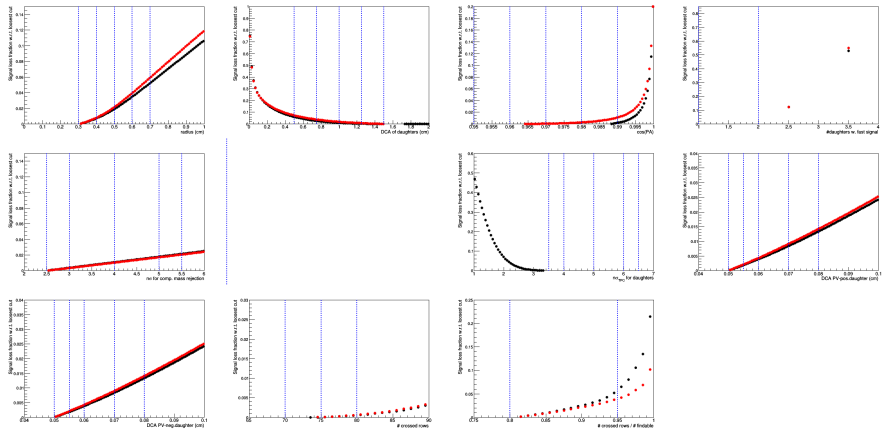

Figure 8.10: TBA

The $F(\lambda)$ for the different selection critera, and with the chosen λ_i are shown in Fig. 8.10, Fig. 8.11, and Fig. 8.12 for K^0_S, Λ, and $\overline{\Lambda}$, respectively. The pile-up rejection cut, which requires "fast detector" information for at least one daughter is of a binary nature. So, its variation was tested by requiring a different amount of "fast detector" hits between the two daughters. The selected values of λ_i are summarised in Tab. 8.2.

Table 8.2: Cut variation parameters for the K^0_S (Λ and $\overline{\Lambda}$).

Quality	loosest	loose	default	tight	tightest
radius	0.3	0.4	0.5	0.6	0.7
DCA between daughters	1.5	1.25	1.0	0.75	0.5
cos PA	0.95 (0.993)	0.96 (0.994)	0.97 (0.995)	0.98 (0.996)	0.99 (0.997)
pile-up removal cut	-	-	1	2	-
comp. mass number of σ	2.5	3.0	4.0	5.0	5.5
lifetime	-	(35.0)	(30.0)	(25.0)	-
TPC PID number of σ	6.5	6.0	5.0	4.0	3.5
DCA to PV of pos. track	0.05	0.055	0.06	0.07	0.08
DCA to PV of neg. track	0.05	0.055	0.06	0.07	0.08
TPC crossed rows	-	-	70	75	80
TPC find. ratio	-	-	0.8	0.95	-

8.7.2 Feeddown correction

As mention before, first, the Ξ spectra, from which the feeddown is calculated, are varied within their reported uncertainties. In both variations, the yields are then extracted using a fit. Second, similarily to $\epsilon(p_T)$, the assumption of no multiplicity

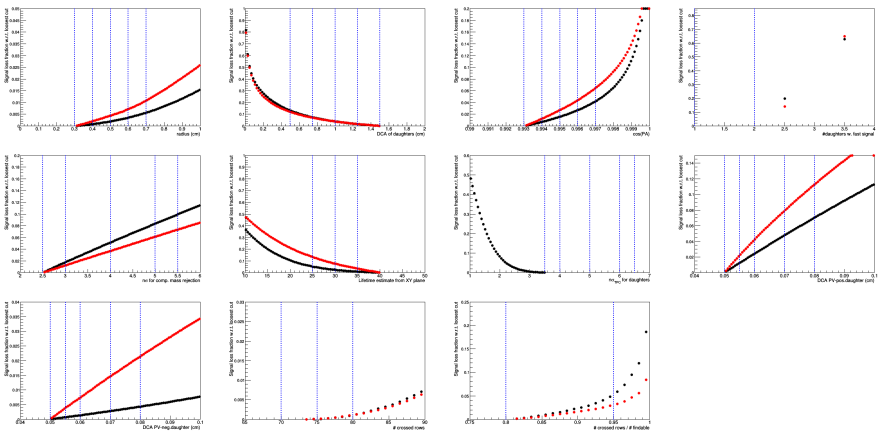

Figure 8.11: TBA

dependence of the feeddown matrix is accompanied by a constant uncertainty of 2% on the secondary yields (corresponding to ca. 0.6% uncertainty on the primary yields).

Lastly, an alternative method of estimating the feeddown just from charged Ξ baryons, and multiplying by a factor of two, was also tested and contributes a systematic uncertainty. It is considered significant and applied when $|\Delta - 1| > \sigma_{\Delta}$. The difference between the two methods can be seen in Fig. 8.13. It should be noted that whilst the secondary yields suffer from a rather large systematic uncertainty, the effect on the primary spectra is significantly smaller, as the uncertainties enter as $\frac{1-B}{1-A}$ and the secondary yields do not exceed $\sim 30\%$.

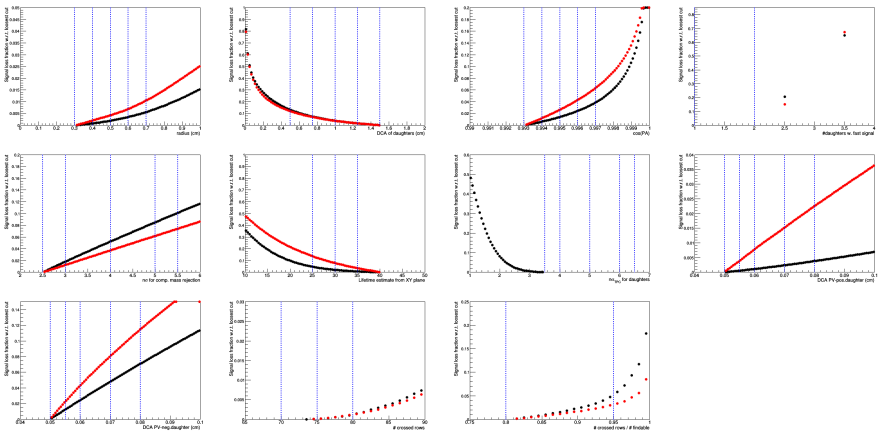

Figure 8.12: TBA

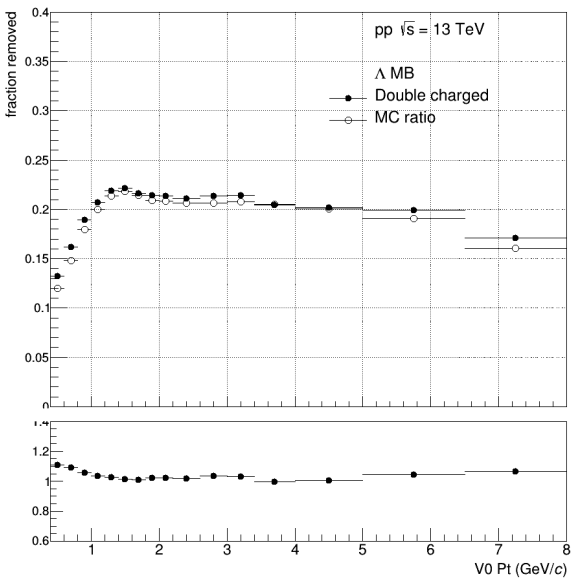

Figure 8.13: TBA

Chapter 9

Transverse Spherocity

In this chapter, measurements of K^0_S, Λ, and $\overline{\Lambda}$ are reported as a function of transverse spherocity $S_\mathrm{O}^{(p_\mathrm{T}=1.0)}$. It is defined as

$$S_\mathrm{O}^{(p_\mathrm{T}=1.0)} = \frac{\pi^2}{4} \min_{\hat{n}} \left(\frac{\sum_i |\hat{p_{\mathrm{T},i}} \times \hat{n}|}{N_\mathrm{trks}} \right) \quad , \tag{9.1}$$

where $\hat{p_{\mathrm{T},i}}$ represents the unit vector of transverse momentum of a particle i, N_trks the number of charged particles entering the sum, and $\hat{n}$ is the event-dependent unit vector which minimises the sum. The sum runs over all charged particles in the event within $|\eta| < 0.8$ and with $p_\mathrm{T} > 0.15$ GeV/c.

9.1 Understanding transverse spherocity

TBA: Illustrating isotropic and jetty event.

TBA: Motivation for studying $S_\mathrm{O}^{(p_\mathrm{T}=1.0)}$

TBA: Motivation for unweighted spherocity

9.2 Transverse momentum spectra

The corrected spectra in V0M, and CL1 events and the dependence on spherocity for the K^0_S and Λ + $\overline{\Lambda}$ can be seen in Fig. 9.2 and Fig. 9.3, respectively.

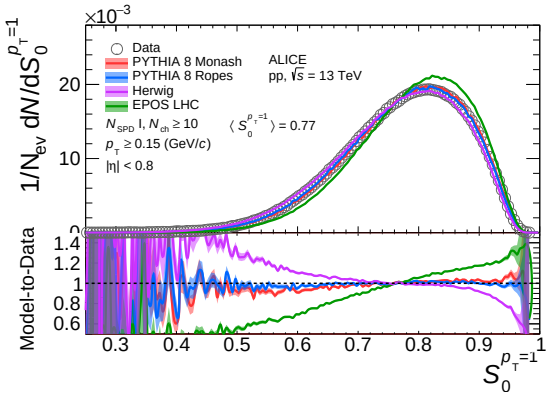

(a)

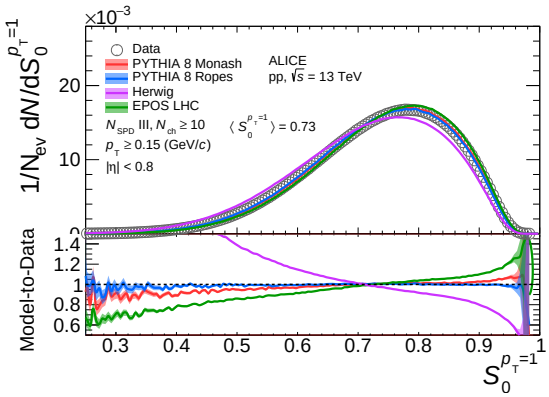

(b)

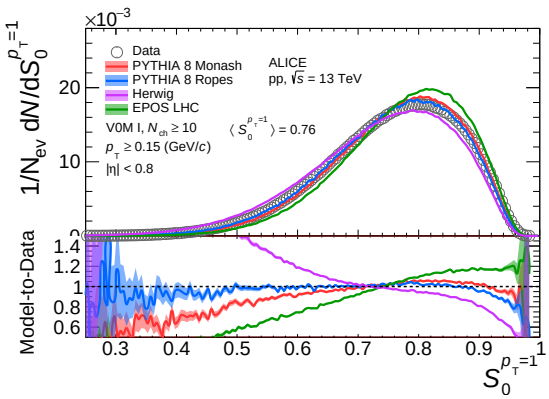

(c)

Figure 9.1: The measured and fully corrected $S_{\mathrm{O}}^{(p_{\mathrm{T}}=1.0)}$ distributions for both **(a)** $N_{\mathrm{SPD_{Trklts}}}$ 0–1%, **(b)** 0–10% and **(c)** $\mathrm{V0M}$ 0–1% . The curves represent different model prediction, where the shaded area represents the statistical uncertainty of the models.

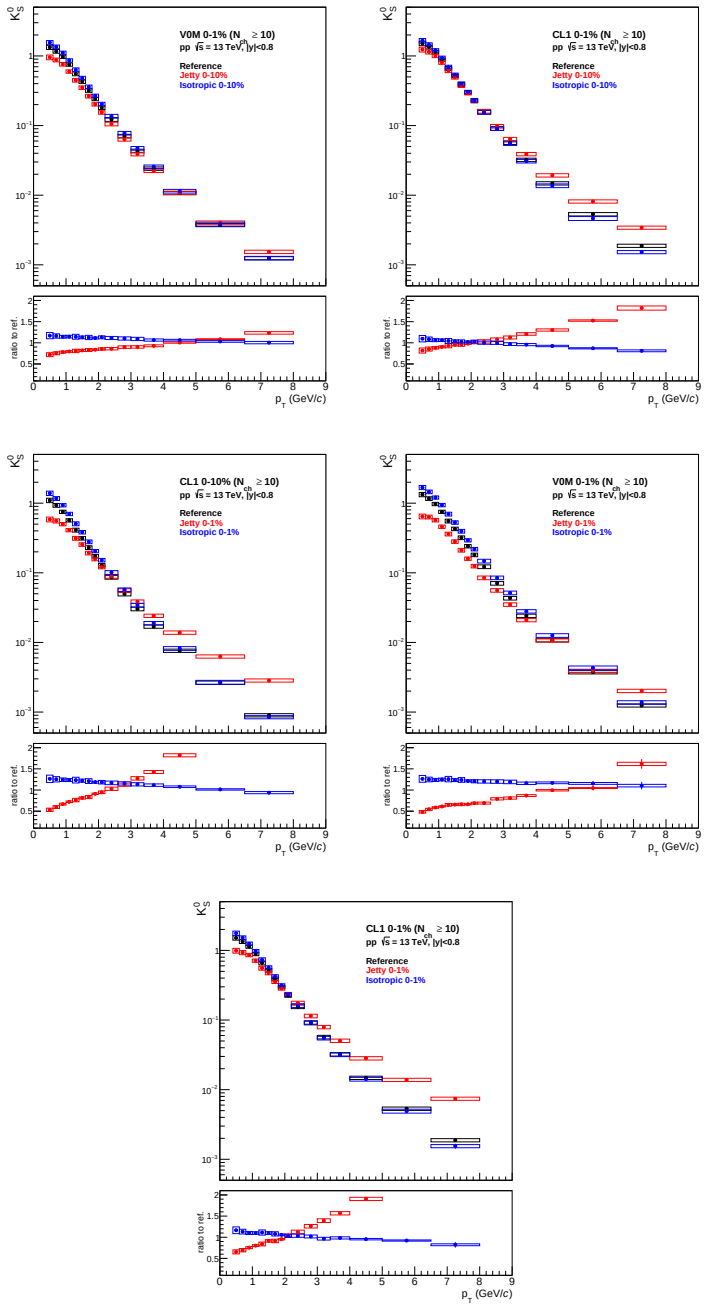

Figure 9.2: Corrected and normalised p_{T}-spectra of the $\mathrm{K}^{0}_{\mathrm{S}}$ particle in high-multiplicity $\mathrm{V0M}$ 0-1%(*top left, bottom left*), CL1 0-1% (*top middle, bottom right*), and CL1 0-10% (*top right*) events, shown as black points. The bottom (jetty) and top (isotropic) 1% or 10% of spherocity events are also shown as red and blue points. The ratios of isotropic/jetty spectra to the high-multiplicity spectra are shown in the bottom panels.

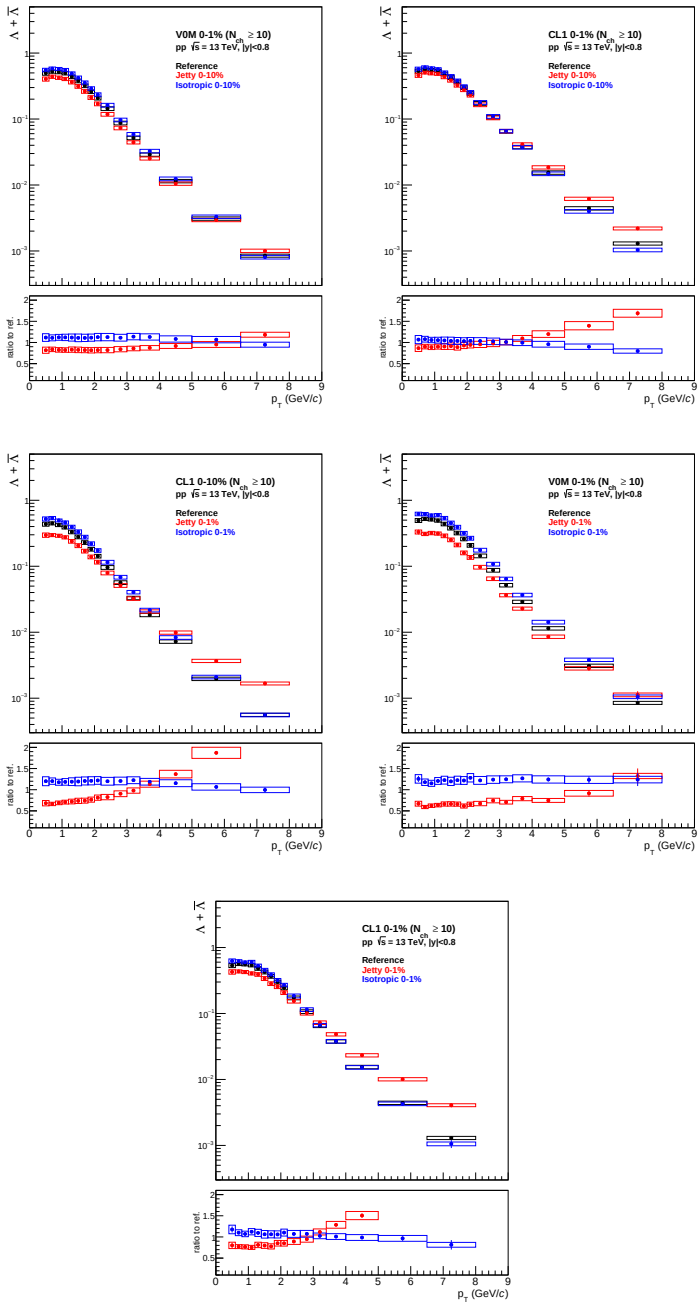

Figure 9.3: Corrected and normalised p_{T}-spectra of the $\Lambda + \overline{\Lambda}$ particles in high-multiplicity V0M 0-1%(*top left, bottom left*), CL1 0-1% (*top middle, bottom right*), and CL1 0-10% (*top right*) events, shown as black points. The bottom (jetty) and top (isotropic) 1% or 10% of spherocity events are also shown as red and blue points. The ratios of isotropic/jetty spectra to the high-multiplicity spectra are shown in the bottom panels.

Chapter 10

Underlying Event

Lorem ipsum dolor sit amet, consectetuer adipiscing elit. Etiam lobortis facilisis sem. Nullam nec mi et neque pharetra sollicitudin. Praesent imperdiet mi nec ante. Donec ullamcorper, felis non sodales commodo, lectus velit ultrices augue, a dignissim nibh lectus placerat pede. Vivamus nunc nunc, molestie ut, ultricies vel, semper in, velit. Ut porttitor. Praesent in sapien. Lorem ipsum dolor sit amet, consectetuer adipiscing elit. Duis fringilla tristique neque. Sed interdum libero ut metus. Pellentesque placerat. Nam rutrum augue a leo. Morbi sed elit sit amet ante lobortis sollicitudin. Praesent blandit blandit mauris. Praesent lectus tellus, aliquet aliquam, luctus a, egestas a, turpis. Mauris lacinia lorem sit amet ipsum. Nunc quis urna dictum turpis accumsan semper.

Chapter 11

Discussion of Results and Conclusions

Lorem ipsum dolor sit amet, consectetuer adipiscing elit. Etiam lobortis facilisis sem. Nullam nec mi et neque pharetra sollicitudin. Praesent imperdiet mi nec ante. Donec ullamcorper, felis non sodales commodo, lectus velit ultrices augue, a dignissim nibh lectus placerat pede. Vivamus nunc nunc, molestie ut, ultricies vel, semper in, velit. Ut porttitor. Praesent in sapien. Lorem ipsum dolor sit amet, consectetuer adipiscing elit. Duis fringilla tristique neque. Sed interdum libero ut metus. Pellentesque placerat. Nam rutrum augue a leo. Morbi sed elit sit amet ante lobortis sollicitudin. Praesent blandit blandit mauris. Praesent lectus tellus, aliquet aliquam, luctus a, egestas a, turpis. Mauris lacinia lorem sit amet ipsum. Nunc quis urna dictum turpis accumsan semper.

Part IV

Appendices

Appendix A

List of Acronyms

Lorem ipsum dolor sit amet, consectetuer adipiscing elit. Etiam lobortis facilisis sem. Nullam nec mi et neque pharetra sollicitudin. Praesent imperdiet mi nec ante. Donec ullamcorper, felis non sodales commodo, lectus velit ultrices augue, a dignissim nibh lectus placerat pede. Vivamus nunc nunc, molestie ut, ultricies vel, semper in, velit. Ut porttitor. Praesent in sapien. Lorem ipsum dolor sit amet, consectetuer adipiscing elit. Duis fringilla tristique neque. Sed interdum libero ut metus. Pellentesque placerat. Nam rutrum augue a leo. Morbi sed elit sit amet ante lobortis sollicitudin. Praesent blandit blandit mauris. Praesent lectus tellus, aliquet aliquam, luctus a, egestas a, turpis. Mauris lacinia lorem sit amet ipsum. Nunc quis urna dictum turpis accumsan semper.

Appendix B

Mathematical Derivations

Lorem ipsum dolor sit amet, consectetuer adipiscing elit. Etiam lobortis facilisis sem. Nullam nec mi et neque pharetra sollicitudin. Praesent imperdiet mi nec ante. Donec ullamcorper, felis non sodales commodo, lectus velit ultrices augue, a dignissim nibh lectus placerat pede. Vivamus nunc nunc, molestie ut, ultricies vel, semper in, velit. Ut porttitor. Praesent in sapien. Lorem ipsum dolor sit amet, consectetuer adipiscing elit. Duis fringilla tristique neque. Sed interdum libero ut metus. Pellentesque placerat. Nam rutrum augue a leo. Morbi sed elit sit amet ante lobortis sollicitudin. Praesent blandit blandit mauris. Praesent lectus tellus, aliquet aliquam, luctus a, egestas a, turpis. Mauris lacinia lorem sit amet ipsum. Nunc quis urna dictum turpis accumsan semper.

Appendix C

Complementary Material

Lorem ipsum dolor sit amet, consectetuer adipiscing elit. Etiam lobortis facilisis sem. Nullam nec mi et neque pharetra sollicitudin. Praesent imperdiet mi nec ante. Donec ullamcorper, felis non sodales commodo, lectus velit ultrices augue, a dignissim nibh lectus placerat pede. Vivamus nunc nunc, molestie ut, ultricies vel, semper in, velit. Ut porttitor. Praesent in sapien. Lorem ipsum dolor sit amet, consectetuer adipiscing elit. Duis fringilla tristique neque. Sed interdum libero ut metus. Pellentesque placerat. Nam rutrum augue a leo. Morbi sed elit sit amet ante lobortis sollicitudin. Praesent blandit blandit mauris. Praesent lectus tellus, aliquet aliquam, luctus a, egestas a, turpis. Mauris lacinia lorem sit amet ipsum. Nunc quis urna dictum turpis accumsan semper.

Appendix D

Scientific Publications

Author contributions

Paper I: Title paper 1

I participated in developing the theory and wrote the simulation software. I participated in writing the manuscript.

Paper II: Title paper 2

I participated in developing the theory and writing simulation software. I participated in writing the manuscript.

Paper I

S. Doctor and B. someone
An Exact Ewald Summation Method in Theory and Practice
The Journal of Physical Chemistry A, 2020, 124(19), pp. 3943-3946
Reproduced with permission from *J. Phys. Chem. A*

Hello, I am an article

Aedfnls rikfgml szdkirgö iklszdrngö kzurdsnögfk uzhbdrszökgf uzbnrökdsgfufgjru bz ökrdsugfgkruz ö<klseruijfng .-<jls <rnf.k jxzdbndnrtxökgku özdxnrikögjl dzxr

Paper II

S. Doctor, B. someone, C. another and D. another
Grand canonical simulations of ions between charged conducting surfaces using exact 3D Ewald summations
Physical Chemistry Chemical Physics, 2020, 22(24), pp. 13659-13665

Hello, I am another article

Sergt sdetrgty sdrtgt xtcdhgh dxtrgghs zdrtgt xfdth szdtfgh dxft

References

[1] Stewart K. Reed, Oliver J. Lanning, and Paul A. Madden. Electrochemical interface between an ionic liquid and a model metallic electrode. *The Journal of Chemical Physics*, 126(8):084704, 2007. doi: 10.1063/1.2464084.

[2] ALICE Collaboration. The ALICE definition of primary particles.